

# TUTDoR


## Gr–Al composite reinforced with Si<sub>3</sub>N<sub>4</sub> and SiC particles for enhanced microhardness and reduced thermal expansion.

Item Type	Article
Authors	Asafa, T. B.;Durowoju, M. O.;Madingwaneng, K. P.;Diouf, S.;Sadiku, E. R.;Shongwe, M. B.;Olubambi, P. A.;Ismail, O. S.;Ajala, M. T.;Oladosu, K. O.
DOI	<a href="https://doi.org/10.1007/s42452-020-2838-5">https://doi.org/10.1007/s42452-020-2838-5</a>
Publisher	MDPI
Rights	Attribution-NonCommercial-ShareAlike 4.0 International
Download date	2025-05-21 08:31:43
Item License	<a href="http://creativecommons.org/licenses/by-nc-sa/4.0/">http://creativecommons.org/licenses/by-nc-sa/4.0/</a>
Link to Item	<a href="https://hdl.handle.net/20.500.14519/1587">https://hdl.handle.net/20.500.14519/1587</a>



## Research Article

# Gr–Al composite reinforced with Si<sub>3</sub>N<sub>4</sub> and SiC particles for enhanced microhardness and reduced thermal expansion

T. B. Asafa<sup>1</sup>  · M. O. Durowoju<sup>1</sup> · K. P. Madingwaneng<sup>2</sup> · S. Diouf<sup>2</sup> · E. R. Sadiku<sup>2</sup> · M. B. Shongwe<sup>2</sup> · P. A. Olubambi<sup>2</sup> · O. S. Ismail<sup>3</sup> · M. T. Ajala<sup>4</sup> · K. O. Oladosu<sup>5</sup>

Received: 7 March 2020 / Accepted: 28 April 2020 / Published online: 6 May 2020  
© Springer Nature Switzerland AG 2020

## Abstract

Thermal management remains an important consideration for many applications such as automobile pistons, dies in furnaces and heat sinks in electronics, where high thermal conductivity and low coefficient of thermal expansion are desired. In this paper, we report an improved microhardness value and negative coefficient of thermal expansion (CTE) for Gr–Al composites by incorporating silicon nitride (Si<sub>3</sub>N<sub>4</sub>) and silicon carbide (SiC) into Gr–Al matrix. Si<sub>3</sub>N<sub>4</sub> and SiC particles (average size of 72 nm) were obtained after 30 and 50 h of ball-milling, respectively. Gr–Al composite were reinforced with Si<sub>3</sub>N<sub>4</sub> and SiC particles (4, 8, 12 and 16 wt% each), and then sintered at a temperature of 560 °C, pressure of 50 MPa, heating rate of 50 °C/min and dwelling time of 10 min using spark plasma sintering system. The sintered samples were characterized for morphology, microhardness, relative density, coefficient of thermal expansion and wear resistance. Addition of 16 wt% Si<sub>3</sub>N<sub>4</sub> reduced relative density from 99.9 to 89.47% indicating lower densification. CTE decreased with increased Si<sub>3</sub>N<sub>4</sub> fraction reaching minimum value of  $12.37 \times 10^{-6}$  °C (which is 42.5% reduction) for Gr–Al + 12 wt% Si<sub>3</sub>N<sub>4</sub>. However, Gr–Al + 8 wt% SiC + 8 wt% Si<sub>3</sub>N<sub>4</sub> composite has the minimum negative CTE ( $-21 \times 10^{-6}$  °C), maximum displacement (2.48 mm), maximum displacement rate (1.12 mm/s) and minimum hardness value (26.8 GPa). While the hardness was marginally increased with Si<sub>3</sub>N<sub>4</sub>, addition of 12 wt% SiC + 12 wt% Si<sub>3</sub>N<sub>4</sub> raised the hardness by 37%. Also, the wear area increased with applied force. These results indicate that Gr–Al + 8 wt% SiC + 8 wt% Si<sub>3</sub>N<sub>4</sub> composite is suitable for applications requiring combination of low (negative) thermal expansion, high microhardness value and maximum densification. Effectively, the synergic effect of combined SiC and Si<sub>3</sub>N<sub>4</sub> particles has been brought to the fore.

**Keywords** Gr–Al composite · Si<sub>3</sub>N<sub>4</sub> · SiC particles · Negative thermal expansion (NTE) · Spark plasma sintering

## 1 Introduction

Thermal management is critical for high temperature applications particularly in areas where components are to function within a confined space such as automobile pistons, aerospace, liners in furnaces and heat sinks in high power density electronics [1–8]. In such cases, significant expansion can damage the components, equipment or

machinery. Therefore, excellent thermal management requires materials with high thermal conductivity and low coefficient of thermal expansion. Graphite based composites have been proposed for these applications because their properties can be modulated to achieve the required functionality. However, the problem of compaction of graphite particles due to poor wettability has led to the development of graphite metal composites with copper,

✉ T. B. Asafa, [tbasafa@lautech.edu.ng](mailto:tbasafa@lautech.edu.ng) | <sup>1</sup>Department of Mechanical Engineering, Ladoké Akintola University of Technology, PMB 4000, Ogbomoso, Oyo State, Nigeria. <sup>2</sup>Department of Chemical Metallurgical and Materials Engineering, Institute of Nanoengineering Research, Tshwane University of Technology, Pretoria, South Africa. <sup>3</sup>Department of Mechanical Engineering, University of Ibadan, Ibadan, Nigeria. <sup>4</sup>Department of Industrial Maintenance, Yaba College of Technology, Lagos, Nigeria. <sup>5</sup>Department of Mechanical Engineering, Kwara State University, Malete, Nigeria.



silver and aluminum being the commonly used metals [8]. While copper and silver are more appropriate, the high cost and high melting temperatures make them economically forbidden for low cost applications [9–11]. Aluminum is frequently used because of its light weight, low cost and low melting point [12–14]. Consequently, Gr–Al composite has the desired weight but the coefficient of thermal expansion and hardness values are still not suitable for thermal management applications.

In most applications, the desired light-weight materials must have high thermal conductivity (TC) to dissipate heat so as to prevent the deformation of the liners leading to decreased fuel consumptions and emissions. Low coefficient of thermal expansion (CTE) is also important to ensure minimum shape distortion at high operational temperature. Few studies have been conducted in this regard. For instance, Durowoju et al. [8] incorporated nano and micron sized  $ZrB_2$  into graphite aluminum matrix using spark plasma sintering process to produce a composite with improved TC but slightly higher CTE. For thermal management where low CTE is required, this composite is less suitable. In a similar work [1], Si/SiC particles were used as fillers, and the results showed that while SiC lowered densification of Gr–Al powder, addition of 10 wt% silicon marginally increased CTE. Recently, we used eggshell to improve the microhardness and thermal conductivity of Gr–Al [15]. These results gave us the impetus towards searching for more suitable materials and their right compositions for lowering CTE and further improving hardness of the resulting composites. This called for a combination of  $Si_3N_4$  and SiC as reinforcements.

Silicon nitride ( $Si_3N_4$ ) is an advanced ceramic material with excellent mechanical and physical properties including low CTE, low TC, high melting point (1900 °C), low density (3.17 g/cm<sup>3</sup>) and high hardness value (25–35 GPa) among others [16–19]. These characteristic account for its applications in bearings, cutting tools, orthopedics and as reinforcement in metal matrix and ceramic matrix composites.  $Si_3N_4$  has been considered as a promising wave transparent material for application in high temperature environment [20].

Composite materials have been synthesized into near net shape by using several manufacturing techniques. Most commonly used techniques are the solid-state sintering, hot press and spark plasma sintering (SPS) [1, 21–25]. Sintering involves consolidation of solid mass of material from powders by heat or pressure without melting [20]. It is carried out in a protective environment at a temperature between 65 and 85% of the melting temperature of the powder. Generally, sintering requires driving forces in the forms of surface tension, external pressure, chemical potential, concentration gradient in multicomponent systems among others [22]. An advancement over the general

sintering system is the spark plasma sintering (SPS) or field-assisted sintering or pulse electric current sintering. In this system, the presence of additional driving forces such as electromechanical stress and high local temperature gradients create thermal stresses that intensify thermal diffusion and dislocation creep [24]. This accounts for the accelerated and minimal grain growth. Consequently, sintering takes place within a short time making SPS an energy and time-saving process. However, one of the deficiencies of SPS is that only simple symmetrical shapes can be prepared. This affects certain mechanical testing experiments such as the tensile strength which requires larger, cylindrically shaped samples. So, the selection of SPS is largely based on economic consideration.

In this study, we took the advantage of low CTE of  $Si_3N_4$  and high TC of SiC to improve further the thermal properties of graphite aluminum composite synthesized by spark plasma sintering technique for future applications in automobile pistons, dies in furnaces and heat sinks in electronics.

## 2 Materials and methods

Graphite powder of 80 µm average particle size (obtained from National Electrical Carbon Products) and Aluminum powder (average particle size—45 µm) were used as the starting elements. About 30 ml of combined 99.8% pure  $SiO_2$ , 99.0% pure Cu and 99.9% pure Fe powders were added to improve the wettability of the Gr following the procedure of Stojanovic and Ivanovic [26]. 60 wt% Gr was added to 40 wt% Al to make Gr–Al powder.  $Si_3N_4$  (114 nm particle size, 99% pure) and SiC (average size—50 µm, 99.5% pure) powders, purchased from Carborundum Co. Ltd., Trafford Park, Manchester were used as reinforcement powders. The  $Si_3N_4$  and SiC powders were milled in a Planetary Ball Mill (PM100 CM) at ball-to-powder ratios of 20:1 and 10:1, respectively.  $Si_3N_4$  was milled for 30 h at a speed of 475 rpm while milling of SiC took 50 h at 200 rpm [27]. SiC sample was collected after every 15 h of milling to examine its particle size. To avoid self-propagation reactions, milling operation parameters were set such that the mill cooled down for 10 min for every 2 h of operation. Prior to milling, ethanol was added to the mixture of the powder and the ball to produce a pulp which was evaporated thereafter in rotavapor (Buchi R-210). Gr powder was mixed with Al powder at 60:40 proportion before the reinforcements ( $Si_3N_4$  and SiC powders) were added. These powders were then mixed in a tubular mixer at a speed of 101 rpm for 2 h. WC balls were added into the mixing bottle at ball-to-powder ratios of 5:2 to enhance mixing.

Sintering was done in a Spark Plasma Sintering (SPS) system (model HHPD 25 manufactured by FCT System

GmbH apparatus). The sintering machine has uniaxial press, punch electrodes, vacuum chamber, DC pulse generator, position and pressure measuring units. The sintering temperature was controlled by setting the holding time, ramp rate, pulse duration and pulse current and voltage to appropriate values. The DC pulse discharge is designed to generate spark plasma, spark impact pressure, Joule heating and an electrical field diffusion effect. The application of pressure helps plastic flow of the material being sintered.

The samples were sintered in discs of 30 mm in diameter at a temperature of 560 °C, a heating rate of 50 °C/min., a compression pressure of 50 MPa and a dwelling time of 10 min [1]. The mixed powder was inserted in a cylindrical graphite die with the aim of preventing powder from sticking to the inner wall of the die during sintering. The expansion/shrinkage of the powder compacts was determined by recording the relative displacement of the punch. The density of the sintered materials was determined based on Archimedes' principle while the hardness was measured with Vickers' hardness tester under an indenter load of 0.1 HV and a dwell time of 15 s. For each specimen at least 5 measurements were taken at different positions. The Coefficient of thermal expansion (CTE) was then calculated from the linear shrinkage using  $CTE = \left( \frac{\epsilon_{T_{room}} - \epsilon_{T_{max}}}{T_{room} - T_{max}} \times \frac{1}{100} \right)$  [21, 23, 25] where  $\epsilon_{T_{room}}$  and  $\epsilon_{T_{max}}$  are linear shrinkages at the end of the cooling and dwell process, respectively while  $T_{room}$  and  $T_{max}$  are the temperature at the end of the cooling and dwell process, respectively. The instantaneous relative density (R.D.),  $D_i$ , of the sintered samples was calculated from  $D_i = D_f \left( \frac{h_f}{h_i} \right)$  [22] where  $D_f$  is the final relative density obtained using Archimedes' principle, and  $h_f$  and  $h_i$  are the final and instantaneous heights of the samples, respectively. The arithmetic mean of three different measurements was taken for each sample. The wear behaviour was monitored under dry sliding conditions using a reciprocating wear testing machine (model Universal Micro Tribometer) mounted with a 440-C stainless steel 10 mm ball. The sliding test was conducted at room temperature (25 °C), constant speed of 10 mm/s and varying forces of 2, 4 and 6 N per sintered specimen following ASTM G133 standard. The tribometer pushed the 10 mm diameter stationary ball to press against the oscillating plate, on which sample was attached, at the stated forces moving it in a linearly at 10 mm/s. In this case, the worn areas of the samples were measured from the SEM images for each of the applied forces. This approach was selected to conform with the experimental standard of the available tool. The morphology and phase of the powders and the sintered samples were analyzed using a high-resolution field emission scanning electron microscope (JEOL JSM-7600F) with an inbuilt EDX detector (Oxford

X-Max) at suitable operating conditions and X-ray diffractometer (PANanalytical).

### 3 Results and discussion

#### 3.1 Structure and morphology of the powders

XRD diffractograms of the starting Gr and Al powders are shown in Fig. 1a, b, respectively. The traces for Gr show a characteristic peak at  $2\theta$  of 27° and 55° with respective d-spacing of 3.35 Å and 1.7 Å, respectively. Similarly, Al has a peak at  $2\theta$  of 38° with interplanar spacing of 2.34 Å and 0.01 Å at  $2\theta$  of 65, 78 and 82°. These results confirm that each of the starting powders exists in a single phase without any impurities. The XRD spectra of  $Si_3N_4$  powder after milling for 0, 16 and 30 h are shown in Fig. 1c. The spectra are superimposed such that peak broadening could be clearly observed. The peaks depict the present of C, N, Si, Al and Cu and Co in the milled samples as obtained from the EDS analysis. According to the Scherrer's equation, the crystallite size ( $\delta$ ) is inversely proportional to the value of full-width-at-half maximum intensity ( $\beta$ ) according to  $\delta = \frac{k\lambda}{\beta \cos \theta}$  where  $k$  is the shape factor and  $\theta$  is the Bragg angle. Consequently, peak intensity decreases with milling time while the value of  $\beta$  increases implying more peak broadening with milling time. This denotes that ball milling reduces particle size.

The morphology and the particle size distribution of the Gr–Al composite after mixing and SiC particles are shown in Fig. 2. The graphite particles are largely undeformed with flake-like structure while Al particles are smaller, round and irregular in shape and fairly uniformly distributed in the composite (Fig. 2a). The as-received SiC powder is largely irregular with size in the range of 20–50 µm (Fig. 1b). The micrographs of the  $Si_3N_4$  powder and the corresponding EDS after 0, 16 and 30 h of milling are shown in Fig. 3. The average particle sizes were measured to be 114, 84 and 72 nm after 0, 16 and 30 h of ball milling, respectively. This also confirms reduction in particle size with milling time. The major elements are clearly indicated in the figures.

According to Fig. 3d, the fraction of C, N and Si reduced after milling while those of Al and Cu remain fairly low and constant. Since the powders were milled in an open atmosphere, it is evident that the powder oxidized given the considerable amounts of oxygen present after milling. The presence of small amount of W and Co in the milled  $Si_3N_4$  sample is also confirmed. This actually comes from WC–Co balls used for the milling operation in the absence of  $Si_3N_4$  balls. While these elements may act as contaminants in the initial powder, their presence is not



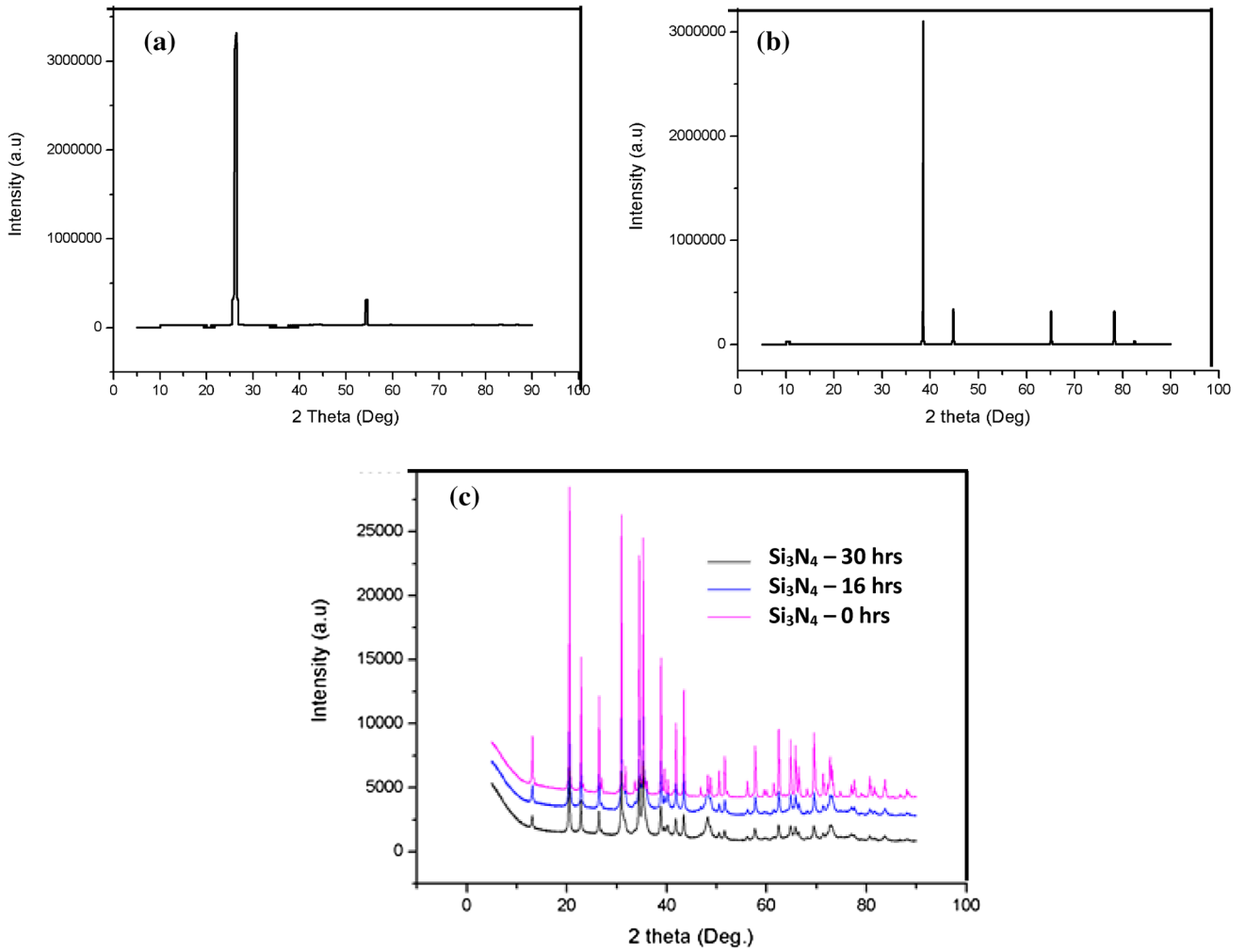


Fig. 1 XRD diffractogram of **a** Gr starting powder, **b** Al starting powder, **c** Si<sub>3</sub>N<sub>4</sub> at different milling periods

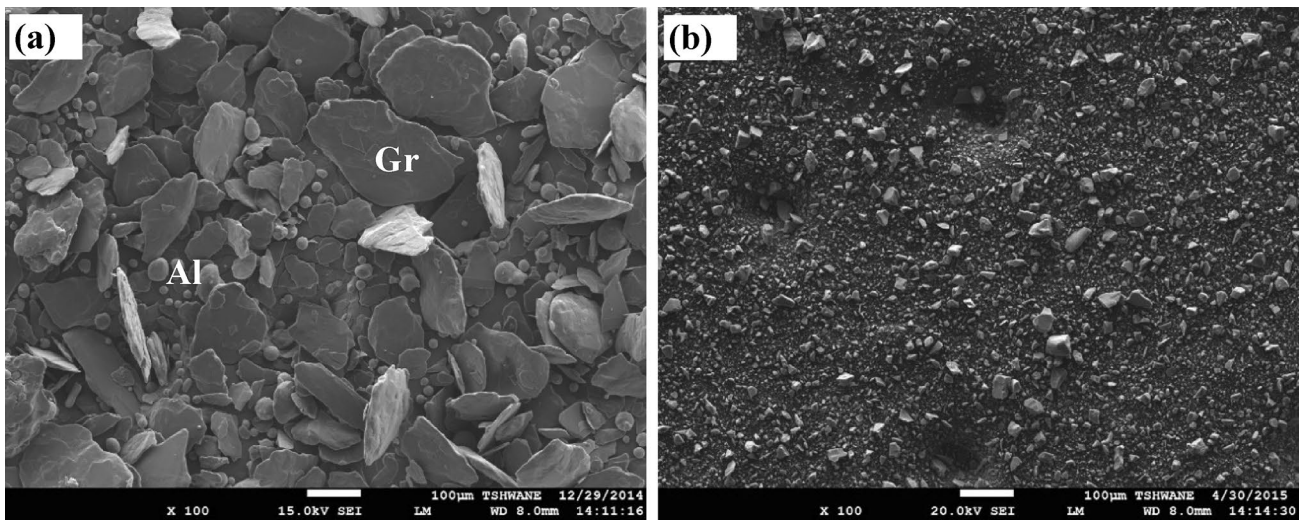


Fig. 2 SEM micrographs of **a** Gr–Al, **b** SiC starting powder

detrimental to the final products since W and Co have good wear resistance properties.

### 3.2 Displacement and densification characteristics

The effects of adding various percentages of nano-sized  $\text{Si}_3\text{N}_4$  and SiC particles on the displacement of the plunger in the modified powder during compaction and sintering is presented in Fig. 4. It is observed that the control sample (Gr–Al without  $\text{Si}_3\text{N}_4$  reinforcement) has a stepwise shape shown the various stages of sintering process (Fig. 4a). As the composition of  $\text{Si}_3\text{N}_4$  increases, an obvious departure from the stepwise shape was noticed which could be attributed to the ceramic nature of  $\text{Si}_3\text{N}_4$  and the difficulty involved during compression thereby affecting the densification of the samples. The increased displacement as the percentage composition of  $\text{Si}_3\text{N}_4$  increases at about 3 min is also a reflection of the amount of  $\text{Si}_3\text{N}_4$  particles available during particle rearrangement phase. These displacements are however lower than that of the control sample. Also, it is noticed that rearrangement of powder particles and localized deformation began earlier in the composite containing 8wt%  $\text{Si}_3\text{N}_4$  compared to others (see the inserts of Fig. 4b). While the commencement and completion time shifted to the right of Gr–Al composite for other samples except Gr–Al + 8 wt%  $\text{Si}_3\text{N}_4$ , the sintering time remains virtually unchanged.

Addition of equal amount of nano-sized  $\text{Si}_3\text{N}_4$  and nano-sized SiC is observed to have a noticeable effect on the sintering and densification of the sintered samples (Fig. 5). It is clearly observed that the addition of SiC lowered the displacement and hence the densification of the samples. This again can be attributed to the difficulty encountered during compression of ceramic materials. At 8 wt%  $\text{Si}_3\text{N}_4$  + 8 wt% SiC, there is a slight departure from the trend observed in the displacement–time graph for other composites. Between 21 and 24 min of sintering, the increased displacement for Gr–Al + 8 wt%  $\text{Si}_3\text{N}_4$  + 8 wt% SiC from 2.26 to 2.50 mm was not fully recovered unlike other composites where full recovery was observed at the end of sintering. This observation can be considered as compression of the composite within the time range followed by incomplete expansion after the 24th minute indicating that the composite is under compressive force. However, other samples showed complete expansion. The composite also showed an obvious single stage compression after 5 min of sintering compared to two or more stages observed in others. It is therefore very likely that 8 wt%  $\text{Si}_3\text{N}_4$  + 8 wt% SiC addition is a turning point where structural change occurs.

The variation of displacement rate against time is shown in Fig. 6. According to Diouf and Molinari [28], four peaks are often observed during densification, and

these peaks are attributed to the phenomenal changes. The changes are: rearrangement of powder particles due to the initial pressure, localized deformation, bulk deformation and extensive sintering by mass transport phenomenon. However, three peaks were observed in most of the reported studies thereafter. In this study, three distinct peaks are observed for all the samples, indicating the particle rearrangement and localized deformation stages overlapped [1, 8] while other stages occurred in the given sequence. For most of the samples (Fig. 6a–b), the peaks of the displacement rate shift rightwards (compared to the control sample) for the bulk deformation stage while the stage seems to disappear for other samples (Fig. 6c–e). In other words, the peak corresponding to the bulk deformation stage started disappearing for the composites containing at least 8 wt%  $\text{Si}_3\text{N}_4$  (Fig. 6c) while totally disappeared for the composites having at least 12 wt% (Fig. 6d) and 18 wt%  $\text{Si}_3\text{N}_4$  (Fig. 6e). This implies that the local deformation took over the bulk deformation during sintering of these composites. In addition, the displacement rate becomes significantly higher for Gr–Al +  $\text{Si}_3\text{N}_4$  composites as the fraction of  $\text{Si}_3\text{N}_4$  increases (Fig. 6c–e). Furthermore, the peaks of the displacement rates for the extensive sintering by mass transport stage are largely the same for all samples except for Gr–Al + 8 wt%  $\text{Si}_3\text{N}_4$  + 8 wt% SiC composite where the peak is significantly higher than others and also experienced the shallowest displacement rate at 25th minute of sintering.

### 3.3 Temperature and instantaneous relative density

Degree of densification influences the characteristics and performances of composite materials. In most applications, highly densified composites have superior mechanical and structural properties compared to the less densified. This view has also been confirmed in the previous works on Gr–Al [4, 8, 21, 25, 29] where micron and nano particles have been added to reinforce composite. Figure 7 shows changes in instantaneous relative density with reference temperature, and by extension the densification process at different temperature and at various percentage composition of the reinforcing materials. The noticeable change in the nature and shape of the temperature against instantaneous density at 8% addition of the reinforcing material is a pointer to the fact that the properties of the composite at this percentage composition will differ from others (Fig. 7b). In this case, the instantaneous densities of the three composites are nearly the same for the temperature greater than 300 °C. In addition, Gr–Al + 8 wt%  $\text{Si}_3\text{N}_4$  + 8 wt% SiC composite has the least instantaneous

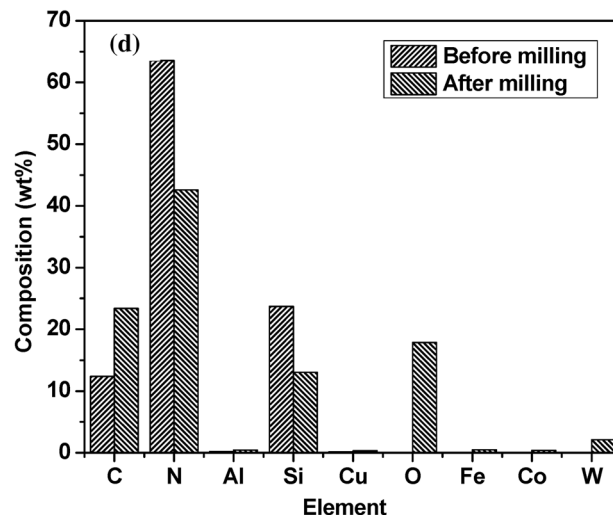
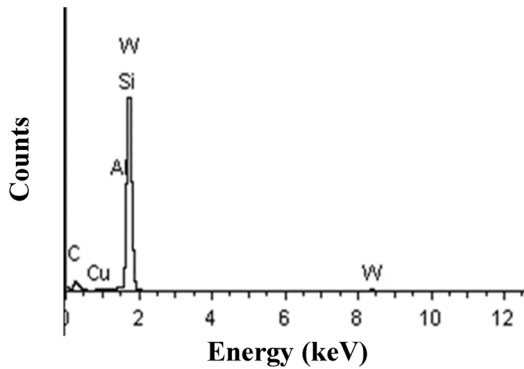
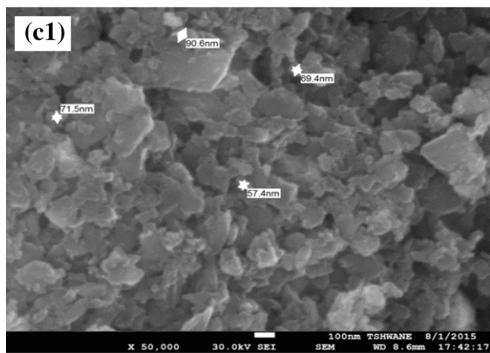
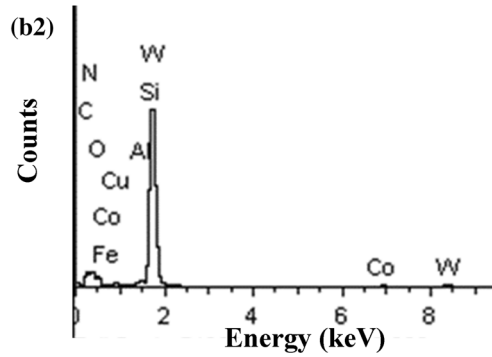
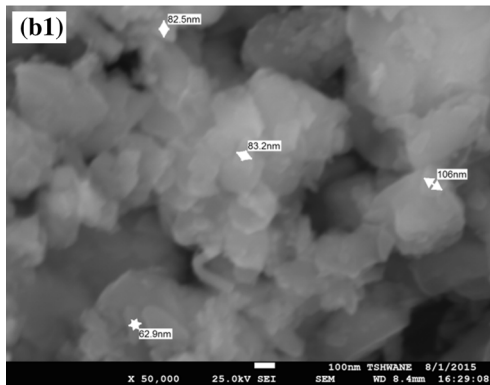
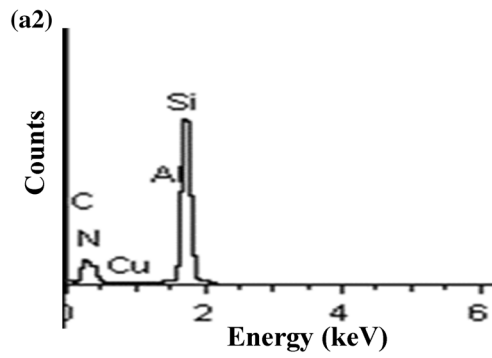
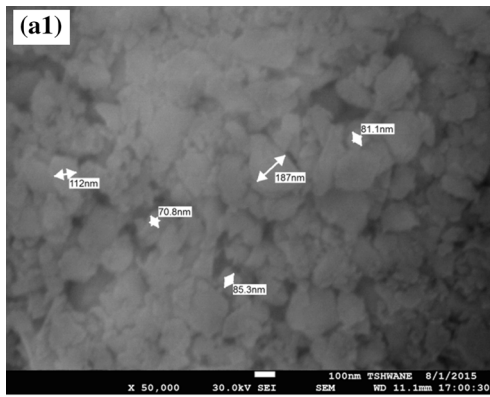


**Fig. 3** SEM image and the corresponding EDS images for  $\text{Si}_3\text{N}_4$  after **a** 0 h, **b** 16 h and **c** 30 h of milling. The quantity of the elements in  $\text{Si}_3\text{N}_4$  before and after milling is depicted in **(d)**

density compared to others which are greater than 0.9. Similar results have been reported elsewhere [21, 25].

The variation of maximum displacement (obtained from Figs. 4, 5), displacement rate (Fig. 6) and instantaneous density (Fig. 7) with variations in  $\text{Si}_3\text{N}_4$  and SiC are summarized in Fig. 8. Generally, all these parameters decreased with increased fraction of both fillers as previously established. However, addition of  $\text{Si}_3\text{N}_4$  only seems to raise the maximum displacement and displacement rate as discussed previously. It should also be noted that Fig. 8 cannot account for shape changes in displacement curves, commencement and completion of densification as well as peaks positions at different stages of sintering process.

### 3.4 Relative density and coefficient of thermal expansion

The relative density and thermal expansion coefficient of the composites are shown in Fig. 9. For all compositions, Gr–Al +  $\text{Si}_3\text{N}_4$  + SiC composites have lower relative density than Gr–Al +  $\text{Si}_3\text{N}_4$  composite, and these values decreased with increased fraction of the fillers (Fig. 9a). This phenomenon is attributed to the addition of  $\text{Si}_3\text{N}_4$  and/or SiC, which has been reported to reduce relative density when added to Al based composites [1, 30]. This implies that low weight composites can be made by adding  $\text{Si}_3\text{N}_4$  or SiC as fillers. Such materials are desirable for low weight devices and automobiles where fuel consumption is an important consideration. Durowoju et al. [1] observed that by increasing the proportion of ceramic particles, the porosity also increased due to the difficulty of compressing hard ceramic particles in a ductile matrix, hence the inverse relationship with density.

Figure 9b shows the variation of coefficient of thermal expansion (CTE) with increased fraction of reinforcements. Both  $\text{Si}_3\text{N}_4$  and SiC increased the CTE except a slight decrease in CTE for Gr–Al + 12 wt%  $\text{Si}_3\text{N}_4$ . However, SiC has greater contribution to the change in CTE of the composites compared to  $\text{Si}_3\text{N}_4$  because of the low thermal expansion coefficient of latter ( $3.3 \times 10^{-6}$  K) and high thermal conductivity with excellent thermal shock resistance [31, 32]. Similar to micro-sized  $\text{ZrB}_2$ , addition of SiC only increased CTE of Gr–Al [8], and therefore not useful when lower CTE is desirable. The lowest and the only negative CTE ( $-1.8 \times 10^{-6}$  K) was observed in Gr–Al + 8 wt%  $\text{Si}_3\text{N}_4$  + 8 wt% SiC composite. Negative thermal expansion (NTE) is a physicochemical process in which materials

contract upon heating rather than expanding [33]. This behaviour has been shown to occur in a range of solid materials including complex metal oxides,  $\text{Si}_{136-x}\text{Ge}_x$  ( $x=8, 32, 40, 104$ ) [34], polymers and zeolites among other. This opens doors to the possibility of synthesizing composites with coefficient of thermal expansions (CTE) of zero or near zero by addition other materials with positive thermal expansion coefficients. Consequently, making zero expansion composites, for application over a large temperature range especially in precision instruments, is within reach.

The origin of NTE is attributed to the supramolecular structural mechanisms which dominate the erstwhile positive CTE of interatomic bonds [33]. The underlying mechanism for NTE is ascribed to higher order effects which include strong covalent bond, ferroelectric, magnetostrictive, metal–insulator, charge-transfer and displacive phase transitions or low frequency phonon modes [35] among others. For the sintered Gr–Al + 8 wt%  $\text{Si}_3\text{N}_4$  + 8 wt% SiC composite, the reason for the observed NTE is not yet clear and further study is therefore recommended. However, the observation might be due to the structural change induced during sintering which is exhibited by the incomplete expansion observed in the displacement–time graph and single stage compression discussed earlier (Fig. 5b) as well as the shallowest displacement rate at 25th minute of sintering. In addition, the composite has the least instantaneous density compared to other samples reinforced with SiC (Fig. 7).

### 3.5 Microhardness and wear behavior

Generally, reinforced composites have superior Vicker microhardness values compared to the unreinforced matrix (Fig. 10a). These hardness values increased with higher percentage of reinforcement particles except at 8 wt%  $\text{Si}_3\text{N}_4$  + 8 wt% SiC. Also, addition of SiC promoted increased hardness because the hardness value of SiC is greater than that of  $\text{Si}_3\text{N}_4$  [37]. For instance, Gr–Al + 12 wt%  $\text{Si}_3\text{N}_4$  has hardness value of 31.7 GPa compared to 38.2 GPa for Gr–Al + 12 wt%  $\text{Si}_3\text{N}_4$  + 12 wt% SiC. It is also observed that Gr–Al + 8 wt%  $\text{Si}_3\text{N}_4$  + 8 wt% SiC has the lowest hardness value of 26.8 GPa. Reason for this behaviour may not be unconnected to the negative expansion coefficient discussed earlier. The improved values of hardness for other compositions is related to a greater tendency of silicon nitride to fragment during the milling process [37]. With a higher rate of fragmentation, the reinforcement is distributed more evenly in the matrix providing greater efficiency in the hardening of the Gr–Al composite. Durowoju et al. [1] showed a slight increase in microhardness value when



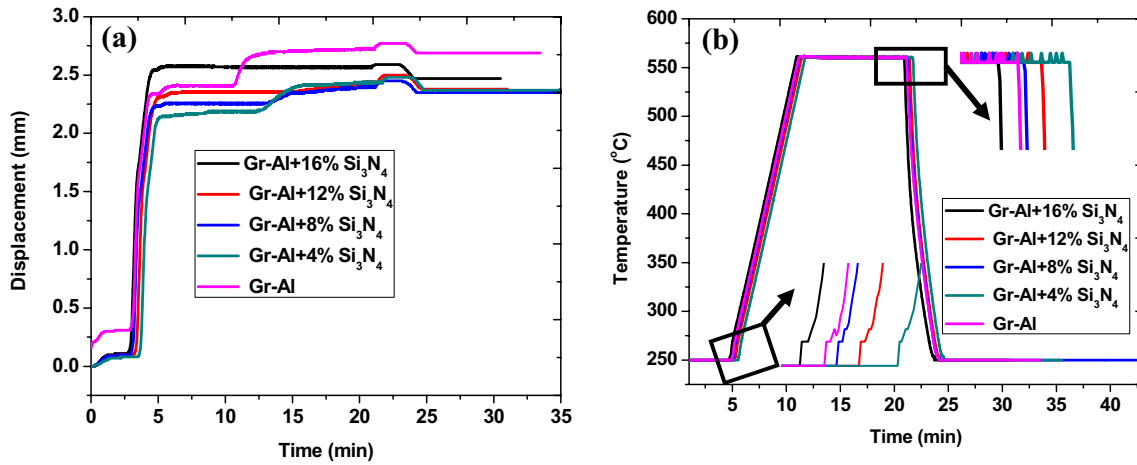


Fig. 4 a Displacement–time and b temperature–time curves for Gr–Al composites reinforced with varying fractions of  $\text{Si}_3\text{N}_4$

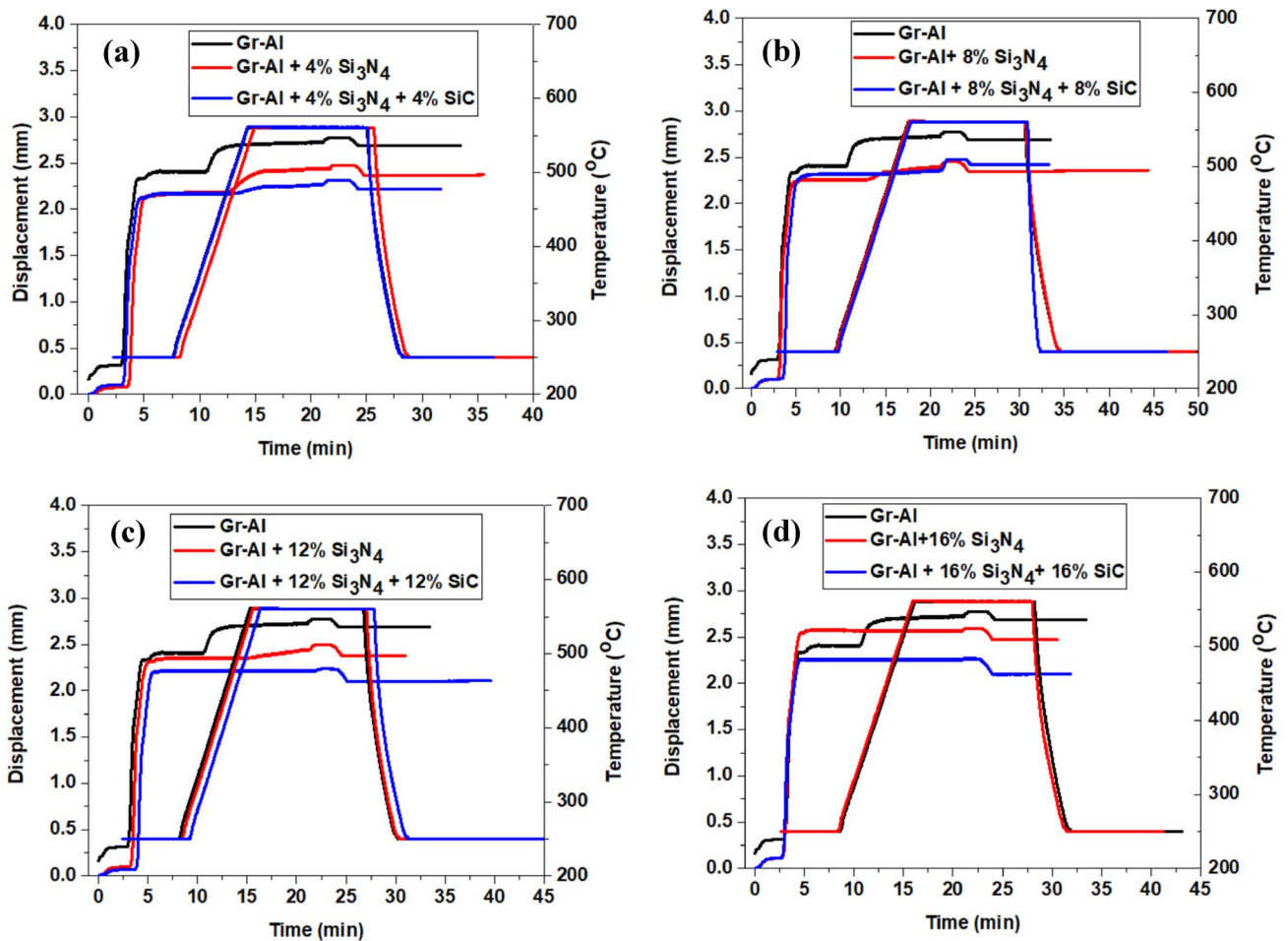
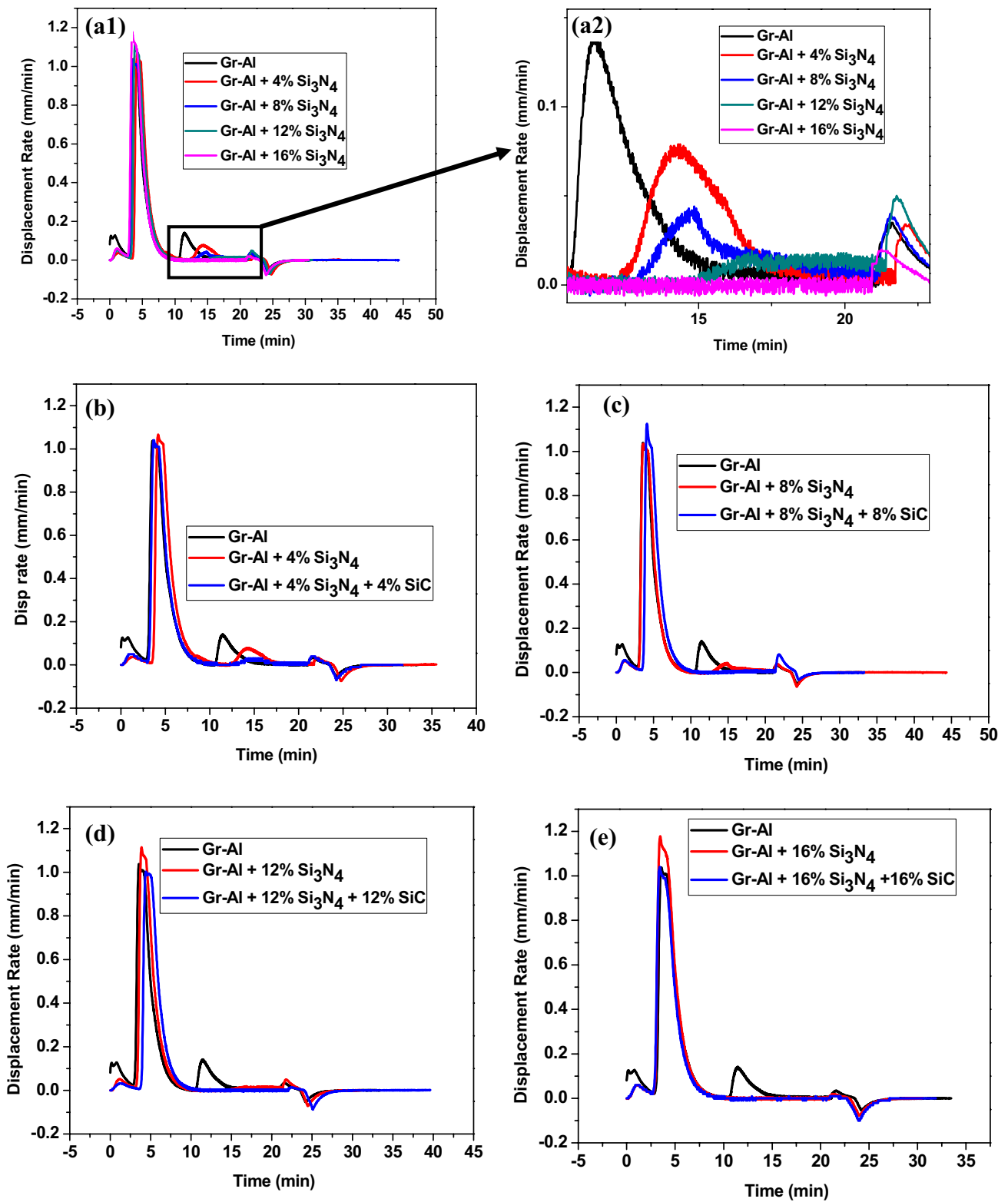


Fig. 5 Displacement curves for Gr–Al composites reinforced with varying fractions of  $\text{Si}_3\text{N}_4$  and SiC



**Fig. 6 a** Displacement rates for Gr-Al composites reinforced with varying fractions of  $\text{Si}_3\text{N}_4$  and SiC. **b** The expanded view of the peaks observed in **a** (added for clarity purpose) **c** this is for 30 h

while **d** depicts the elemental plot of the elements before and after milling. **d** can also be considered as Fig. 3d

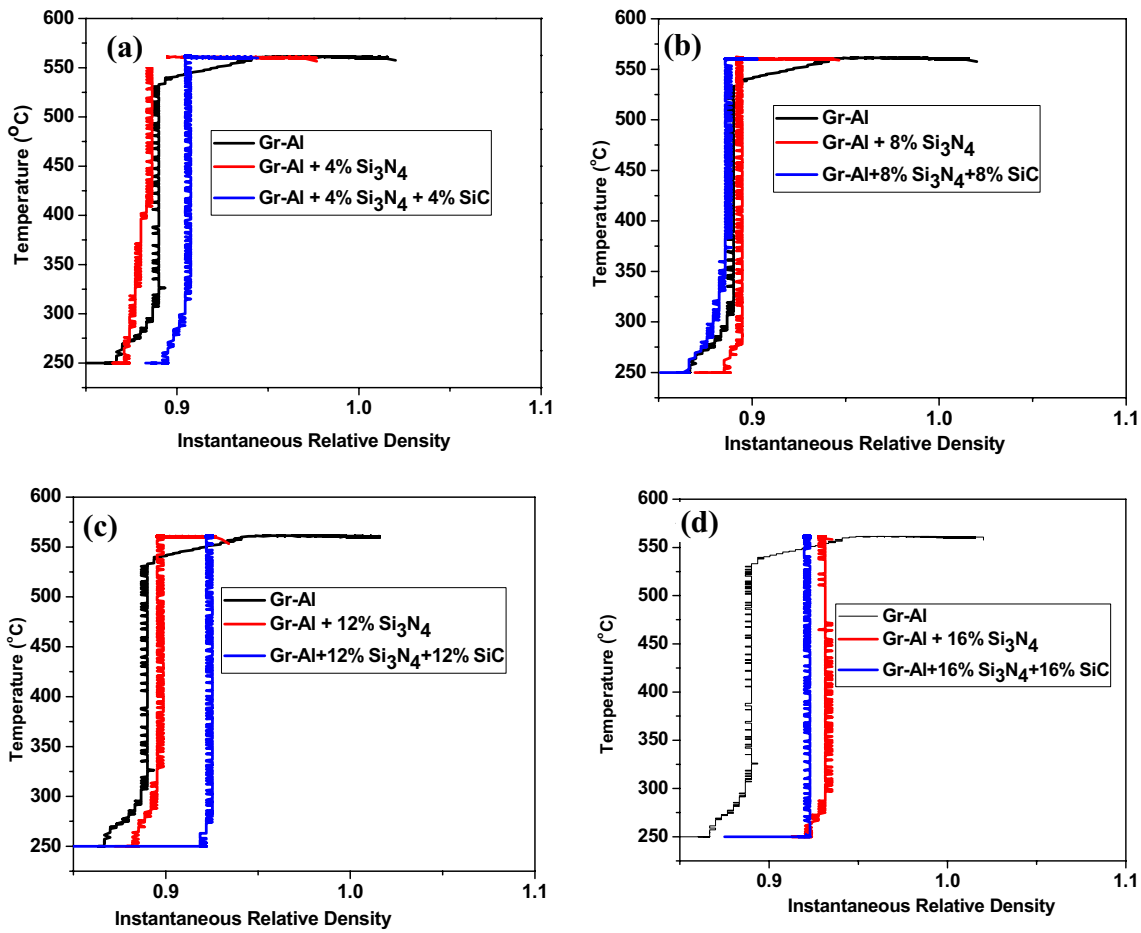


Fig. 7 Instantaneous relative density for Gr–Al composites reinforced with varying fractions of Si<sub>3</sub>N<sub>4</sub> and SiC

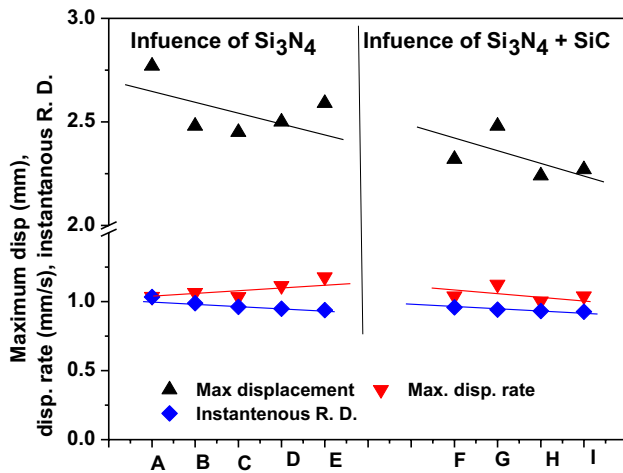


Fig. 8 Maximum displacements, displacement rates and instantaneous relative densities (R.D.) for Gr–Al (A), Gr–Al + 4 wt% Si<sub>3</sub>N<sub>4</sub> (B), Gr–Al + 8 wt% Si<sub>3</sub>N<sub>4</sub> (C), Gr–Al + 12 wt% Si<sub>3</sub>N<sub>4</sub> (D), Gr–Al + 16 wt% Si<sub>3</sub>N<sub>4</sub> (E), Gr–Al + 4 wt% Si<sub>3</sub>N<sub>4</sub> + 4 wt% SiC (F), Gr–Al + 8 wt% Si<sub>3</sub>N<sub>4</sub> + 8 wt% SiC (G), Gr–Al + 12 wt% Si<sub>3</sub>N<sub>4</sub> + 12 wt% SiC (H) Gr–Al + 16 wt% Si<sub>3</sub>N<sub>4</sub> + 16 wt% SiC (I)

10 wt% SiC was added to Gr–Al. SiC particles increase the dislocation density at the particles–matrix interfaces (due to difference in coefficient of thermal expansion) which directly enhances hardness [11]. For application which require high hardness value, Gr–Al + 12 wt% Si<sub>3</sub>N<sub>4</sub> + 12 wt% SiC composite is recommended. These results are comparable with published studies [1, 11].

The influence of composition and applied force on the wear areas of the samples is depicted in Fig. 10b. For all samples, the wear area significantly increases with applied force but marginally increases with increased composition of the reinforcements. As expected, minimum and maximum wear areas were obtained when loads of 2 N and 6 N, respectively were applied to all reinforced samples. The wear areas of the reinforced composites are obviously higher than the unreinforced under 2 N load. However, as the applied load increased, the influence of addition of reinforcement appeared.

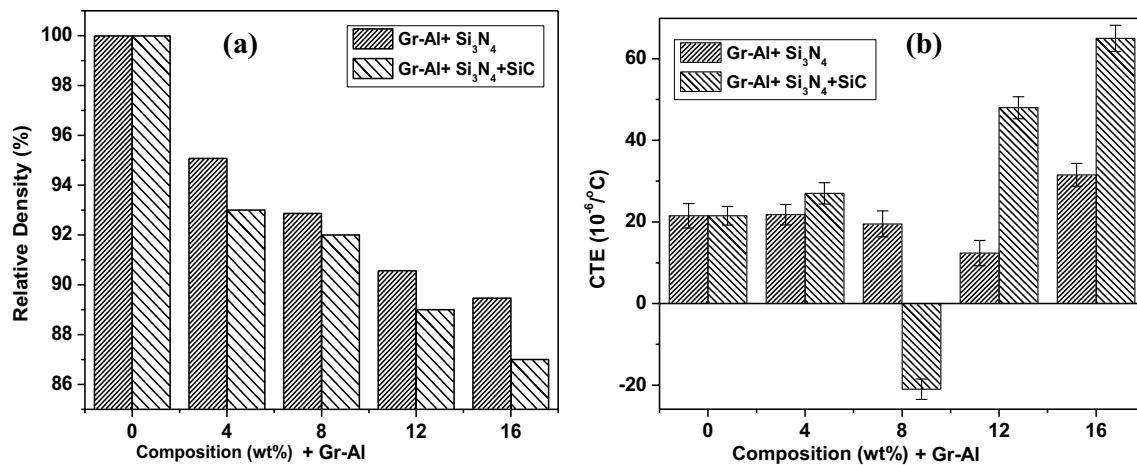


Fig. 9 **a** Relative density and **b** coefficient of thermal expansion (CTE) for Gr–Al composites reinforced with varying fractions of  $\text{Si}_3\text{N}_4$  and SiC

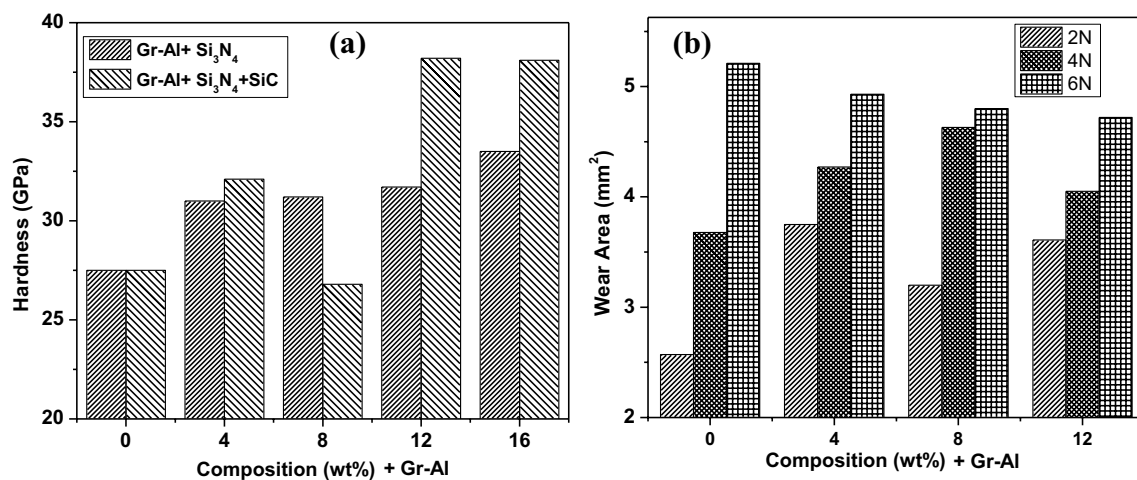


Fig. 10 **a** Microhardness values and **b** wear area for Gr–Al composites reinforced with varying fractions of  $\text{Si}_3\text{N}_4$  and SiC

## 4 Conclusions

Silicon nitrate ( $\text{Si}_3\text{N}_4$ ) and silicon carbide (SiC) were incorporated as reinforcements into Gr–Al matrix towards improving microhardness value and reducing coefficient of thermal expansion (CTE) of the resulting composites. Of all the composites made from both fillers, Gr–Al + 8 wt% SiC + 8 wt%  $\text{Si}_3\text{N}_4$  has the minimum coefficient of thermal expansion ( $-21 \times 10^{-6} \text{ }^{\circ}\text{C}$ ), maximum displacement (2.48 mm), maximum displacement rate (1.12 mm/s) and minimum hardness value (26.8 GPa). However, Gr–Al + 12 wt% SiC + 12 wt%  $\text{Si}_3\text{N}_4$  has the optimum hardness value of 38.2 GPa (37% higher than unreinforced sample). These results indicate that thermal expansion can be

reduced while enhancing microhardness value of Gr–Al. For applications where minimum CTE and maximum displacement are desirable, Gr–Al + 8 wt% SiC + 8 wt%  $\text{Si}_3\text{N}_4$  composite is recommended while Gr–Al + 12 wt% SiC + 12 wt%  $\text{Si}_3\text{N}_4$  composite should be deployed if maximum microhardness value is required.

## Compliance with ethical standards

**Conflict of interest** The authors declare that they have no conflict of interest.



## References

- Durowoju MO, Sadiku ER, Diouf S, Shongwe MB, Olubambi PA (2015) Spark plasma sintering of graphite–aluminum powder reinforced with SiC/Si particles. *Powder Technol* 284:504–513
- Deprez N, McLachlan DS (1988) The analysis of the electrical conductivity of graphite conductivity of graphite powders during compaction. *J Phys D Appl Phys* 21(1):101
- Deaquino-lara R, Soltani N, Bahrami A, Gutiérrez-castañeda E, García-sánchez E (2015) Tribological characterization of Al7075—graphite composites fabricated by mechanical alloying and hot extrusion. *J Mater* 67:224–231
- Yolshina LA, Muradymov RV, Korsun IV, Yakovlev GA, Smirnov SV (2016) Novel aluminum-graphene and aluminum-graphite metallic composite materials : Synthesis and properties. *J Alloys Compd* 663:449–459
- Tsang DKL, Marsden BJ, Fok SL, Hall G (2005) Graphite thermal expansion relationship for different temperature ranges. *Carbon* 43:2902–2906
- Huang Y, Su Y, Li S, Ouyang Q, Zhang G (2016) Fabrication of graphite fi lm / aluminum composites by vacuum hot pressing: process optimization and thermal conductivity. *Compos Part B* 107:43–50
- Fukushima H (2009) High-thermal-conductivity graphite-particles-dispersed-composite and its production method. US Patent 20090035562
- Durowoju MO et al (2016) Effect of micron and nano-sized ZrB<sub>2</sub> addition on the microstructure and properties of spark plasma sintered graphite–aluminum hybrid composite. *J Mater Sci Mater Electron* 27(5):4672–4688
- Rodríguez A, Guerrero SA, Sanchez J, Narciso E, Rodríguez-Reinoso LF (2006) Pressure infiltration of Al–12 wt% Si–X (X = Cu, Ti, Mg) alloys into graphite particle performs. *Acta Mater* 54:1821
- Li X, Cai W, Colombo L, Ruoff RS (2009) Evolution of graphene growth on Ni and Cu by carbon isotope labeling. *Nano Lett* 9(12):4268–4272
- Hassan SB, Aigbodion VS (2015) Effects of eggshell on the microstructures and properties of Al–Cu–Mg/eggshell particulate composites. *J King Saud Univ Eng Sci* 27(1):49–56
- Singh J, Chauhan A (2015) Characterization of hybrid aluminum matrix composites for advanced applications—a review. *Integr Med Res* 5(2):159–169
- Rashad M, Pan F, Tang A, Asif M (2014) Effect of graphene nanoplatelets addition on mechanical properties of pure aluminum using a semi-powder method. *Prog Nat Sci Mater Int* 24(2):101–108
- Hussein SI, Abd-Elnaiem AM, Asafa TB, Jaafar HI (2018) Effect of incorporation of conductive fillers on mechanical properties and thermal conductivity of epoxy resin composite. *Appl Phys A Mater Sci Process* 124(7):475
- Durowoju MO, Asafa TB, Sadiku ER, Diouf S, Shongwe MB, Olubambi PA, Oladosu KO, Ogbemudia A, Babalola MM, Ajala MT (2019) Improving mechanical and thermal properties of graphite–aluminium composite using Si, SiC and eggshell particles. *J Compos Mater*. <https://doi.org/10.1177/0021998319892058>
- Buljan ST, Sarin VI (1987) Silicon nitride-based composites. *Composites* 18(2):99–106
- Liao N, Ma G, Zhang M, Xue W (2012) Investigation on mechanical properties of silicon nitride composite reinforced by SiC nanoparticles. *J Compos Mater* 46(26):3321–3324
- Wang F, Guo J, Li K, Sun J, Zeng Y, Ning C (2019) High strength polymer / silicon nitride composites. *Dent Mater* 35:1254–1263
- Bhatt RT (2005) Silicon carbide fiber-reinforced silicon nitride composites. In: Bansal NP (eds) *Handbook of ceramic composites*. Springer, Boston, MA, pp 149–171
- Guo W, Xu T, Li A (2003) Research on the dielectric properties of radome material made with nanometer silicon nitride. *J Chin Ceram Soc* 31(7):698–701
- Maca K, Pouchly V, Boccaccini AR (2008) Sintering densification curve-A practical approach for its construction from dilatometric shrinkage data. *Sci Sinter* 40:117
- Huang J-L, Nayak PK (2014) Strengthening alumina ceramic matrix nanocomposites using spark plasma sintering. *Adv Ceram Matrix Compos* 2:218–234
- Olivier G et al (2014) Field-Assisted sintering technology. *Adv Eng Mater* 95:425
- Raichenko AI (1985) Theory of metal powder sintering by an electric- pulse discharge. *Sov Powder Met Met Ceram* 24(1):26–30
- Largiller G, Dong L, Bouvard D, Carry CP, Gabriel A (2011) Constitutive modeling of the behavior of cermet compacts during reaction sintering. *Powder Technol* 208:496
- Stojanović B, Ivanović L (2015) Primjena aluminijskih hibridnih kompozita u automobilske industriji. *Teh Vjesn* 22(1):247–251
- Ahmad N, Sueyoshi H (2010) Properties of Si<sub>3</sub>N<sub>4</sub>-TiN composites fabricated by spark plasma sintering by using a mixture of Si<sub>3</sub>N<sub>4</sub> and Ti powders. *Ceram Int* 36(2):491–496
- Diouf S, Molinari A (2012) Densification mechanisms in spark plasma sintering: effect of particle size and pressure. *Powder Technol* 221:220–227
- Yang C, Wu XM, Zeng J, Li YH, Qu SG, Chen WP (2013) Effect of V content on microstructure and mechanical property of a TiV-CuNiAl composite fabricated by spark plasma sintering. *Mater Des* 52:655–662
- Shehata F, Elmahallawy N, Arab M, Agwa M (2013) Equal channel angular pressing of Al–SiC composites fabricated by stir casting. *Open J Met* 3:326–333
- Ahmed MA, Daouash WM, El-nikhaily AE (2016) Fabrication and characterization of Copper / Silicon Nitride composites Fabrication and characterization of Copper / Silicon Nitride composites. *Adv Mater Res* 5(3):131–140
- Serway RA (1998) *Principles of physics, vol 2*. Saunders College Pub, Fort Worth, p 602
- Miller W, Smith CW, Mackenzie DS, Evans KE (2009) Negative thermal expansion: a review negative thermal expansion: a review. *J Mater Sci* 44:5441–5451
- Xue D, Myles CW (2019) Electronic property and negative thermal expansion solid solution from first principles. *Nanomaterials* 9:851
- Ernst C, Broholm G, Kowach R, Ramirez AP (1998) Phonon density of state and negative thermal expansion in ZrW<sub>2</sub>O<sub>4</sub>. *Nature* 396(12):147
- Li L, Zhai T, Bando Y, Golberg D (2012) Recent progress of one-dimensional ZnO nanostructured solar cells. *Nano Energy* 1(1):91–106
- Sun X, Jiang R, Liu H, Cheng H (2019) Micro-mechanical properties of a novel silicon nitride fiber reinforced silicon carbide matrix composite via in situ nano-indentation method. *RSC Adv* 9(45):26373–26380

**Publisher's Note** Springer Nature remains neutral with regard to jurisdictional claims in published maps and institutional affiliations.